

## ABUNDANCE GRADIENTS AND THE ROLE OF SNE IN M87

FABIO GASTALDELLO

IASF - CNR, via Bassini 15, I-20133 Milano, Italy

Università di Milano Bicocca, Dip. di Fisica, P.za della Scienza 3 I-20133 Milano, Italy

gasta@ifctr.mi.cnr.it

AND

SILVANO MOLENDI

IASF - CNR, via Bassini 15, I-20133 Milano, Italy

silvano@ifctr.mi.cnr.it

to appear in *ApJ*

## ABSTRACT

We make a detailed measurement of the metal abundance profiles and metal abundance ratios of the inner core of M87/Virgo observed by *XMM-Newton* during the PV phase. We use multi temperature models for the inner regions and we compare the plasma codes APEC and MEKAL. We confirm the strong heavy elements gradient previously found by *ASCA* and *BeppoSAX*, but also find a significant increase in light elements, in particular O. This fact together with the constant O/Fe ratio in the inner 9 arcmin indicates an enhancement of contribution in the core of the cluster not only by SNIa but also by SNII.

*Subject headings:* X-rays: galaxies — Galaxies: clusters — Galaxies: individual: M87 — Galaxies: abundances

## 1. INTRODUCTION

The X-ray emitting hot intra-cluster medium (ICM) of clusters of galaxies is known to contain a large amount of metals: for rich clusters between red-shift 0.3-0.4 and the present day the observed metallicity is about 1/3 the solar value (Mushotzky & Lowenstein 1997; Fukazawa et al. 1998; Allen & Fabian 1998; Della Ceca et al. 2000; Etti et al. 2001), suggesting that a significant fraction of the ICM has been processed into stars already at intermediate red-shifts.

While the origin of the metals observed in the ICM is clear (they are produced by supernovae), less clear is the transfer mechanism of these metals to the ICM. The main mechanisms that have been proposed for the metal enrichment in clusters are: enrichment of gas during the formation of the proto-cluster (Kauffman & Charlot 1998); ram pressure stripping of metal enriched gas from cluster galaxies (Gunn & Gott 1972; Tonazzo & Schindler 2001); stellar winds AGN- or SN-induced in Early-type galaxies (Matteucci & Vettolani 1988; Renzini 1997).

Spatially resolved abundance measurement in galaxy clusters are of great importance because they can be used to measure the precise amounts of metals in the ICM and to constrain the origin of metals both spatially and in terms of the different contributions of the two different type of SNe (SNII and SNIa) as a function of the position in the cluster. The first two satellites able to perform spatially resolved spectroscopy, *ASCA* and *BeppoSAX* have revealed abundance gradients in cD clusters (Dupke & White 2000b; De Grandi & Molendi 2001), in particular M87/Virgo (Matsumoto et al. 1996; Guainazzi & Molendi 2000), and variations in Si/Fe within a cluster (Finoguenov et al. 2000) and among clusters (Fukazawa et al. 1998). Since the SNIa products are iron enriched, while the SNII products are rich in  $\alpha$  elements, such as O, Ne, Mg and Si, the variations in Si/Fe suggest that the metals in the ICM have been produced by a mix of the two types of SNe. The exact amount of these mix still remain controversial: Mushotzky et al. (1996) and

Mushotzky & Lowenstein (1997) showed a dominance of SNII ejecta, while other works on *ASCA* data (Ishimaru & Arimoto 1997; Fukazawa et al. 1998; Finoguenov et al. 2000; Dupke & White 2000a), still indicating a predominance of SNII enrichment at large radii in clusters, do not exclude that as much as 50% of the iron in clusters come from SNIa ejecta in the inner part of clusters.

M87 is the cD galaxy of the nearest cluster and its high flux and close location allows, using the unprecedented combination of spectral and spatial resolution and high throughput of the EPIC experiment on board *XMM-Newton*, a detailed study of the ICM abundance down to the scale of the kpc. Throughout this paper, we assume  $H_0 = 50 \text{ km s}^{-1} \text{ Mpc}^{-1}$ ,  $q_0 = 0.5$  and at the distance of M87 1' corresponds to 5 kpc.

Recently, when we were finishing the writing of the paper, we have learned of the Finoguenov et al (2001) analysis of the same data. Our work is complementary with theirs in the sense that we use 10 annular bins instead of 2, fully exploiting the quality of the *XMM* data and taking into account the multi temperature appearance of spectra in the inner regions with adequate spectral modeling.

The outline of the paper is as follows. In section 2 we give information about the *XMM* observation and on the data preparation. In section 3 we suggest the use of a unique set of “standard” abundances. In section 4 we describe our spectral modeling. In section 5 we present spatially resolved measurements of metal abundances and abundance ratios and in section 6 we discuss our results. A summary of our conclusions is given in section 7.

## 2. OBSERVATION AND DATA PREPARATION

M87/Virgo was observed with *XMM-Newton* (Jansen et al. 2001) during the PV phase with the MOS detector in Full Frame Mode for an effective exposure time of about 39 ks. Details on the observation have been published in Böhringer et al. (2001) and Belsole et al. (2001). We have obtained calibrated event files for the MOS1 and MOS2 cameras with SASv5.0. Data

were manually screened to remove any remaining bright pixels or hot column. Periods in which the background is increased by soft proton flares have been excluded using an intensity filter: we rejected all events accumulated when the count rates exceeds 15 cts/100s in the [10 – 12] keV band for the two MOS cameras.

We have accumulated spectra in 10 concentric annular regions centered on the emission peak extending our analysis out to 14 arcmin from the emission peak, thus exploiting the entire *XMM* field of view. We have removed point sources and the substructures which are clearly visible from the X-ray image (Belsole et al. 2001) except in the innermost region, where we have kept the nucleus and knot A, because on angular scales so small it is not possible to exclude completely their emission. We prefer to fit the spectrum of this region with a model which includes a power law component to fit the two point like sources. We include only one power law component due to the similarity of the two sources spectra (Böhringer et al. 2001). The bounding radii are 0'-0.5', 0.5'-1', 1'-2', 2'-3', 3'-4', 4'-5', 5'-7', 7'-9', 9'-11' and 11'-14'. The analysis of the 4 central regions within 3 arcmin was already discussed in Molendi & Gastaldello (2001).

Spectra have been accumulated for MOS1 and MOS2 independently. The Lockman Hole observations have been used for the background. Background spectra have been accumulated from the same detector regions as the source spectra.

The vignetting correction has been applied to the spectra rather than to the effective area, as is customary in the analysis of EPIC data (Arnaud et al. 2001). Spectral fits were performed in the 0.5-4.0 keV band. Data below 0.5 keV were excluded to avoid residual calibration problems in the MOS response matrices at soft energies. Data above 4 keV were excluded because of substantial contamination of the spectra by hotter gas emitting further out in the cluster, on the same line of sight.

As discussed in Molendi (2001) there are cross-calibration uncertainties between the spectral response of the two EPIC instruments, MOS and PN. In particular for what concern the soft energy band (0.5-1.0 keV) fitting six extra-galactic spectra for which no excess absorption is expected, MOS recovered the  $N_H$  galactic value, while PN gives smaller  $N_H$  by  $1 - 2 \times 10^{20} \text{cm}^{-2}$ . Thus we think that at the moment the MOS results are more reliable than the PN ones in this energy band, which is crucial for the O abundance measure. For this reason and for the better spectral resolutions of MOS, which is again important in deriving the O abundance, we limit our analysis to MOS data.

### 3. SOLAR ABUNDANCES

The elemental abundances of astrophysical objects are usually expressed by the relative values to the solar abundances. The so-called solar abundances can be either “meteoritic” or “photospheric”.

This distinction between “meteoritic” and “photospheric” solar abundances was made in the review by Anders & Grevesse (1989). Significant discrepancies exist between the two sets of abundances quoted in that paper, particularly for iron and this has caused in the past some controversy in the discussion of the results of cluster abundances (Ishimaru & Arimoto 1997; Gibson et al. 1997). However recent photospheric models of the sun indicate that photospheric and meteoritic abundances agree perfectly and the community has converged toward a “standard solar composition” (Grevesse & Sauval 1998), with suggestions to the astrophysical community to accept this new state

of the art (Brighenti & Mathews 1999). For the above reason, in this paper we shall adopt the Grevesse & Sauval (1998) values. Since the solar abundance table used by default in XSPEC is based on photospheric values of Anders & Grevesse (1989), we have switched to a table taken from the data by Grevesse & Sauval (1998) by means of the XSPEC command ABUND. In general a simple scaling allows to switch from one set of abundances to the other.

### 4. SPECTRAL MODELING AND PLASMA CODES

All spectral fitting has been performed using version 11.0.1 of the XSPEC package.

All models discussed below include a multiplicative component to account for the galactic absorption on the line of sight of M87. The column density is always fixed at a value of  $1.8 \times 10^{20} \text{cm}^{-2}$ , which is derived from 21cm measurements (Lieu et al. 1996). Leaving  $N_H$  to freely vary does not improve the fit and does not affect the measure of the oxygen abundance, which could have been the more sensitive to the presence of excess absorption. The  $N_H$  value obtained is consistent within the errors with the 21cm value.

The temperature profile for M87 (Böhringer et al. 2001) shows a small gradient for radii larger than  $\sim 2$  arcmin and a rapid decrease for smaller radii. Moreover, as pointed out in Molendi & Pizzolato (2001) all spectra at radii larger than 2 arcmin are characterized by being substantially isothermal (although the spectra of the regions between 2 and 7 arcmin are multi temperature spectra with a narrow temperature range rather than single temperature spectra), while at radii smaller than 2 arcmin we need models which can reproduce the broad temperature distribution of the inner regions.

We therefore apply to the central regions (inside 3 arcmin) three different spectral models.

A two temperature model (vmekal + vmekal in XSPEC and model II in Molendi & Gastaldello (2001) using the plasma code MEKAL (Mewe et al. 1985; Liedahl et al. 1995). This model has 15 free parameters: the temperature and the normalization of the two components and the abundance of O, Ne, Na, Mg, Al, Si, S, Ar, Ca, Fe and Ni, all expressed in solar units. The metal abundance of each element of the second thermal component is bound to be equal to the same parameter of the first thermal component. This model is used (e.g. Makishima et al. (2001) and refs. therein) as an alternative to cooling-flow models in fitting the central regions of galaxy clusters.

A “fake multi-phase” model (vmekal + vmcflow in XSPEC and model III in Molendi & Gastaldello (2001). This model has 15 free parameters, as the two temperature model, because the maximum temperature  $T_{max}$  is tied to the vmekal component temperature. As indicated in recent papers (Molendi & Pizzolato 2001; Molendi & Gastaldello 2001) this model is used to describe a scenario different from a multi-phase gas, for which it was written for: the gas is all at one temperature and the multi-phase appearance of the spectrum comes from projection of emission from many different physical radii. A more correct description will be given by a real deprojection of the spectrum (Pizzolato et al., in preparation).

The third model is the analogue of the vmekal two temperature model using the plasma code APEC (Smith et al. 2001). This model has 14 free parameters, one less than the corresponding model using vmekal because APEC misses the Na parameter.

We can't adopt an APEC analogue of the fake multi-phase

model because the cooling flow model calculating its emission using APEC is still under development. Given the substantial agreement between 2T and fake multi-phase model (Molendi & Gastaldello 2001), we can regard the 2T APEC results as indicative also for a fake multi-phase model.

For the spectrum accumulated in the innermost region we included also a power law component to model the emission of the nucleus and of knot A.

For the outer regions (from 3 arcmin outwards) we apply single temperature models: vmekal using the MEKAL code, with 13 free parameters and vpec using the APEC code, with 12 free parameters.

As pointed out by the authors of the new code, cross-checking is very important, since each plasma emission code requires choosing from a large overlapping but incomplete set of atomic data and the results obtained by using independent models allows critical comparison and evaluation of errors in the code and in the atomic database.

## 5. RESULTS

### 5.1. Abundance measurements and modeling concerns

The X-ray emission in cluster of galaxies originates from the hot gas permeating the cluster potential well. The continuum emission is dominated by thermal bremsstrahlung, which is proportional to the square of the gas density times the cooling function. From the shape and the normalization of the spectrum we derive the gas temperature and density. In addition the X-ray spectra of clusters of galaxies are rich in emission lines due to K-shell transitions from O, Ne, Mg, Si, S, Ar and Ca and K- and L-shell transitions from Fe and Ni, from which we can measure the relative abundance of a given element.

In Figure 1 we show the data of the 3'-4' bin together with the best fitting model calculated using the MEKAL code. The model has been plotted nine times, each time all element abundances, except one, are set to zero. In this way the contribution of the various elements to the observed lines and line blends become apparent. In the energy band (0.5-4 keV) we have adopted for the spectral fitting, the abundance measurements based on K-lines for all the elements except for Fe and Ni, for which the measure is based on L-lines. The K-lines of O, Si, S, Ar and Ca are well isolated from other emission features and clearly separated from the continuum emission, which are the requirements for a robust measure of the equivalent width of the lines and consequently of the abundances of these elements. The Fe-L lines are known to be problematic, because the atomic physics involved is more complicated than K-shell transitions (Liedahl et al. 1995), but from the very good signal of *XMM* spectra and from the experience of *ASCA* data (Mushotzky et al. 1996; Hwang et al. 1997; Fukazawa et al. 1998) we can conclude that the Fe-L determination is reliable. Some of the stronger Fe-L lines due to Fe XXII and Fe XXIV are close to the K-lines of Ne and Mg, respectively and blending can lead to errors in the Ne abundance and, to a smaller extent, to the Mg abundance (Liedahl et al. 1995; Mushotzky et al. 1996). Also the Ni measure is difficult due to the possible confusion of its L-lines with the continuum and Fe-L blend.

### 5.2. Abundance profiles

In Figure 2 we report the MOS radial abundance profiles for O (top panel), Si (middle panel) and Fe (bottom panel), in Figure 3 those for Mg (top panel), Ar (middle panel) and S (bottom panel), in Figure 4 those for Ne (top panel), Ca (middle panel)

and Ni (bottom panel). We note that the measurements obtained using the two different plasma codes agree for what concerns Fe, Ar and Ca; they are somewhat different for what concerns O, S and Ni and in complete disagreement for Mg and Ne.

The temperature profile obtained with the two codes is showed in Figure 5: there are some differences in the inner regions, while in the outer isothermal bins there is substantially agreement.

The models using the APEC code give a systematically worse description than the ones using MEKAL code: for the multi temperature models with APEC the  $\chi^2$  range from 403 to 498 for  $\nu = 218$  (216 in the central bin due to the two additional degree of freedom of the power-law component), while for MEKAL models (2T and fake multi-phase give the same results) the  $\chi^2$  range from 323 to 382 for  $\nu = 217$  (215 in the central bin due to the two additional degree of freedom of the power-law component); for single temperature models with APEC the  $\chi^2$  range from 546 to 886 for  $\nu = 222$ , while for MEKAL models the  $\chi^2$  range from 326 to 731 for  $\nu = 221$ . In Figure 6 we compare the residuals in the form of  $\Delta\chi^2$  between a 2T model using the MEKAL code and the APEC code for the inner bin 1'-2', as well as a 1T model using the MEKAL code and the APEC code for the "isothermal" bins 3'-4' and 11'-14'. It's evident that in the external bins the differences in the fit between the two codes are due to APEC over-prediction of the flux of Fe-L lines from high ionization states, considering the fact that the temperature obtained by the two codes are nearly coincident. For the inner regions the differences between the two codes are further complicated by the different temperature range they find for the best fit. In general, where the temperature structure is very similar, as in the innermost bin, the difference is as in the outer bins in the high energy part of the Fe-L blend, while where the temperature structure is different, as in the 1'-2' shown in Figure 6, the differences between the two codes are primary due to different estimates of the flux of He-like Si-K line.

We therefore choose as our best abundance profiles those obtained with a 2T vmekal fit for the central regions and with a 1T vmekal fit for the outer regions. In Table 1 we report the abundance profiles for O, Ne, Na, Mg, Al, Si, S, Ar, Ca, Fe and Ni obtained in this way. Abundance gradients are clearly evident for Fe, Si, S, Ar and Ca; O, Mg and Ni show evidence for an enhancement in the central regions while only Ne is substantially flat.

### 5.3. Comparison with Finoguenov et al. (2001) results

We made a direct comparison of our results with the abundances and abundance ratios derived by Finoguenov et al (2001). Their values are consistent within the errors with ours except for the oxygen abundance, which is roughly two times higher in Finoguenov's analysis. To better understand the origin of this discrepancy we have extracted spectra from the same radial bins, 1'-3' and 8'-14', and fitted a single temperature model (vmekal) in the 0.5-10 keV band, excising the 0.7-1.6 keV energy range, in order to avoid the dependence from the Fe L-shell peak, as done by Finoguenov et al (2001). Our results for the O abundance, given in units of the solar values from Anders & Grevesse (1989) to make a direct comparison with the results of Table 1 of Finoguenov et al (2001), are  $0.32 \pm 0.03$  for the 1'-3' bin and  $0.20 \pm 0.02$  for the 8'-14' bin, to be compared with  $0.535^{+0.019}_{-0.021}$  and  $0.386^{+0.025}_{-0.021}$ . Also interesting are the results for the Ni abundance:  $2.55 \pm 0.33$  for the 1'-3' bin and

$2.34 \pm 0.26$  for the 8'-14' bin, to be compared with  $2.573^{+0.924}_{-0.918}$  and  $0.800^{+1.732}_{-0.800}$ . We also note that a 2T modeling of the inner bin 1'-3' gives a statistically better fit over a single temperature model ( $\chi^2/\text{d.o.f}$  of 919/440 respect to 1083/442, using the 0.5-10 keV band) breaking down the assumption of near isothermality.

We also cross compare the K- and L-shell results for Ni and Fe in our analysis, performing the spectral fits for all the radial bins in the 0.5-10 keV band, but excising the 0.7-1.6 keV energy range. The derived abundances for the two elements are consistent within  $1\sigma$ , although the K-shell Ni abundance is 20% higher than the L-shell abundance in the bins fitted with a single temperature model. It should be borne in mind that particularly for the outer bins the K-shell Ni abundance measure is very sensitive to the background estimate.

#### 5.4. Abundance ratios and SNIa Fe mass fraction

From the abundance measurements we obtain the abundance ratios between all the elements relative to Fe, normalized to the solar value. They are shown in Figure 7, Figure 8, Figure 9 and in Table 2, together with the abundance ratios obtained by models of supernovae taken by Nomoto et al. (1997) and rescaled to the solar abundances reported in Grevesse & Sauval (1998). We use those abundance ratios to estimate the relative contributions of SNIa and SNII to the metal enrichment of the intra-cluster gas. Such estimates are complicated by uncertainties both in the observations and in the theoretical yields. Our approach is to use the complete set of ratios trying to find the best fit of the function

$$\left(\frac{X/Fe}{X_{\odot}/Fe_{\odot}}\right)_{\text{observed}} = f \left(\frac{X/Fe}{X_{\odot}/Fe_{\odot}}\right)_{\text{SNIa}} + (1-f) \left(\frac{X/Fe}{X_{\odot}/Fe_{\odot}}\right)_{\text{SNII}} \quad (1)$$

where  $\left(\frac{X/Fe}{X_{\odot}/Fe_{\odot}}\right)_{\text{observed}}$  is the measured abundance ratio of the X element to Fe, given in solar units,  $\left(\frac{X/Fe}{X_{\odot}/Fe_{\odot}}\right)_{\text{SNIa}}$  and  $\left(\frac{X/Fe}{X_{\odot}/Fe_{\odot}}\right)_{\text{SNII}}$  are the theoretical abundance ratio by the two types of supernovae, also given in solar units and  $f$  is directly the SNIa Fe mass fraction. The result of the simultaneous fit of the eight ratios is presented as circles in Figure 10, using the SNII model by Nomoto et al. (1997) and W7, WDD1 and WDD2 models for SNIa respectively for the three panels. Due to the large uncertainties in the yields for the SNII model, the results are strongly SNII model dependent. For comparison we use the range of SNII yields calculated by Gibson et al. (1997), also listed in Table 2, which involve only ratios for O, Ne, Mg, Si and S and as before finding the best fit for eq.(1). The results are shown as squares for the lower end of the range and triangles for the upper part of the range.

The best fits are obtained in the inner bins with a combination of the WDD2 model for SNIa and the Nomoto model for SNII, with reduced  $\chi^2$  which ranges from 2 in the inner bin up to 10 in the 4'-5' bin. In the outer bins the fit is slightly better (reduced  $\chi^2$  of 8-10 instead of 12-13) with a combination of the W7 model for SNIa and the Nomoto model for SNII. This is shown in Figure 11 where the fits with the three SNIa models together with the Nomoto SNII model are reported for the 0.5'-1' bin and for the 11'-14' bin. It's clear from the inspection of the residuals in terms of  $\Delta\chi^2$  that the combination of W7 model and Nomoto SNII model fails in the inner bins because it predicts a higher Ni/Fe and O/Fe ratio, compared to the de-

layed detonation models. The situation is the opposite for the outer bins where a higher Ni/Fe and a lower S/Fe favors the W7 model. However the preference for the W7 model in combination with the Nomoto SNII model in the outer bins is strongly dependent on the Ni/Fe ratio: if we exclude it from the fit the WDD2 model provides the better fit to the data.

## 6. DISCUSSION

The model emerging from the *ASCA* and *BeppoSAX* data for the explanation of abundance gradients in galaxy clusters was that of a homogeneous enrichment by SNII, the main source of  $\alpha$  elements, maybe in the form of strong galactic winds in the proto-cluster phase and the central increase in the heavy element distribution due to an enhanced contribution by SNIa, strongly related to the presence of a cD galaxy (Fukazawa et al. 1998; Dupke & White 2000b; Finoguenov et al. 2000; De Grandi & Molendi 2001; Makishima et al. 2001). As a textbook example we can consider the case of A496 observed by *XMM-Newton* (Tamura et al. 2001). The O-Ne-Mg abundance is radially constant over the cluster, while the excess of heavy elements as Fe, Ar, Ca and Ni in the core is consistent with the assumption that the metal excess is solely produced by SNIa in the cD galaxy. The crucial ratio for the discrimination of the enrichment by the two types of supernovae, O/Fe, is then decreasing towards the center.

The *XMM* results for M87/Virgo question this picture. They confirm and improve the accuracy of the measure of heavy elements gradients previously found by *ASCA* and *BeppoSAX*, but they also show a statistically significant enhancement of  $\alpha$  elements O and Mg in the core. If we consider the inner 9 arcmin the ratio O/Fe is constant with  $\chi^2 = 6.9$  for 7 d.o.f. and adding a linear component does not improve the fit ( $\chi^2 = 5.4$  for 6 d.o.f). These facts point toward an increase in contribution also of SNII, since O is basically produced only by this kind of supernovae. Although there is little or no evidence of current star formation in the core of M87, the O excess could be related to a recent past episode of star formation triggered by the passage of the radio jet, as we see in cD galaxies with a radio source (A1795 cD: van Breugel et al. 1984 and A2597 cD: Koekemoer et al. 1999), nearby (Cen A: Graham 1998) and distant radio galaxies (van Breugel et al. 1985; van Breugel & Dey 1993; Bicknell et al. 2000) (for a comprehensive discussion see McNamara 1999).

To put the above idea quantitatively, waiting for a true deprojection of our data, we use previous *ROSAT* estimate of the deprojected electron density in the center of the Virgo cluster (Nulsen & Böhringer 1995) to calculate the excess mass of oxygen. To estimate the excess abundance we fit the inner bins, where we see the stronger increase in the O abundance, with a constant obtaining an abundance of 0.32, while for the outer bins we obtain an abundance of 0.21 so the excess is 0.11. Then we estimate the oxygen mass,  $M_O$  to be  $M_O = A_O y_{O,\odot} Z_O^{\text{excess}} M_H$ , where  $M_H = 0.82 n_e \frac{4\pi}{3} (R_{\text{out}} - R_{\text{in}})^3$ ,  $R_{\text{in}}$  and  $R_{\text{out}}$  being the bounding radii in kpc of the bins,  $A_O = 16$  and  $y_{O,\odot} = 6.76 \times 10^{-5}$  from Grevesse & Sauval (1998). We obtain a rough estimate of  $10^7 M_{\odot}$  which, assuming that about  $80 M_{\odot}$  of star formation are required to generate a SNII (Thomas & Fabian 1990) and Nomoto SNII oxygen yield, requires a cumulative star formation of  $4 - 5 \times 10^7 M_{\odot}$ . This star formation is in agreement with a burst mode of star formation ( $\lesssim 10^7$  yr) at rates of  $\sim 10 - 40 M_{\odot} \text{ yr}^{-1}$ , as it is observed in the CD galaxies of A1795 and A2597 (McNamara 1999).

For what concern heavy element gradients and the contribution of SNIa, M87 data suggests an agreement with delayed detonation models (in particular for the inner bins), as stressed by Finoguenov et al (2001), in contrast with the preference of W7 model set by the high Ni/Fe ratios found by Dupke & White (2000a). This is particular evident if we consider the S/Fe ratio in Figure 7. If we consider the set of theoretical values for SNII and W7 SNIa models the behavior of these ratio would indicate an increasing contribution by SNIa going *outward* to the center. We recover the correct behavior if we choose the WDD1 yield and we reduce the S SNII yield of Nomoto et al. (1997) by a factor of two to three, as was already indicated by ASCA data (Dupke & White 2000a). We caution however that this is a substantial contribution larger than that allowed by the SNII models choosed by Gibson et al. (1997). The use of delayed detonation model for SNIa could also explain the over abundance of S and also Si (respect to the W7 model) found by Tamura et al. (2001) for the core of A496.

With increasing radius the W7 model gives a better fit to the data respect to delayed detonation models. This fact indicates a SNIa abundance pattern change with radius and could be taken as an independent X-ray confirmation of the conclusions of Hatano et al. (2000) on the optical spectroscopic diversity of SNIa, as suggested by Finoguenov et al (2001). However we stress that the preference of W7 over WDD models in the outer bins is entirely due to the Ni/Fe ratio which could be affected by systematic uncertainties, as discussed in section 5.1 and 5.3.

In Figure 10, we show the relative importance of SNIa, measured by the Fe mass fraction provided by this kind of supernovae. This is substantially constant through the 14 arcmin analyzed. This fraction is considerable and ranges between the 50% and 80% and it depends only slightly on the SNIa model used. Instead the uncertainties involved in using different SNII models are large and a definitive answer cannot be reached until further convergence of SNII models is achieved.

## 7. SUMMARY

We have performed a spatially resolved measurement of the element abundances in M87, the Virgo cluster cD galaxy. The main conclusion of our work are:

- the APEC code gives a systematically worse description than the MEKAL code in modeling M87 spectra;
- we confirm the increase of Fe and other heavy elements towards the core indicating that the SNIa contribution increases;
- the increase in O abundance and a constant O/Fe ratio in the inner 9 arcmin indicates an increase also in SNII ejecta possibly from star-burst in the recent past;
- Si/Fe and S/Fe profiles favor WDD models over W7, also requiring substantial reduction of the SNII yield of S;
- the indication of a change of the SNIa abundance pattern, provided by a preference of the W7 model over delayed detonation models in the outer bins, is entirely due to the Ni/Fe ratio. Since the Ni measurement is difficult and uncertain, this indication should be taken with some caution.

S. Ettori and S. Ghizzardi are thanked for useful discussions and suggestions. We thank the referee for several suggestions that improved the presentation of this work. This work is based on observations obtained with *XMM-Newton*, an ESA science mission with instruments and contributions directly funded by ESA Member States and the USA (NASA).

## REFERENCES

- Allen, S. W. & Fabian, A. C. 1998, *MNRAS*, 297, L63  
 Anders, E. & Grevesse, N. 1989, *Geochimica et Cosmochimica Acta*, 53, 197  
 Arnaud, M., Neumann, D. M., Aghanim, N., Gastaud, R., Majerowicz, S., Hughes, J. P. 2001, *A&A*, 365, L80  
 Belsole, E., Sauvageot, J. L., Böhringer, H., Worrall, D. M., Matsushita, K., Mushotzky, R. F., Sakelliou, I., Molendi, S., Ehle, M., Kennea, J., Stewart, G., Vestrand, W. T. 2001, *A&A*, 365, L188  
 Bicknell, G., Sutherland, R., van Breugel, W.J.M., Dopita, M.A., Dey, A., Miley, G.K. 2000, *ApJ*, 540, 678  
 Böhringer, H., Belsole, E., Kennea, J., Matsushita, K., Molendi, S., Worrall, D. M., Mushotzky, R. F., Ehle, M., Guainazzi, M., Sakelliou, I., Stewart, G., Vestrand, W. T., Dos Santos, S. 2001, *A&A*, 365, L181  
 Brighenti, F. & Mathews, W. G. 1999, *ApJ*, 515, 542  
 De Grandi, S. & Molendi, S. 2001, *ApJ*, 551, 153  
 Della Ceca, R., Scaramella, R., Gioia, I. M., Rosati, P., Fiore, F., Squires, G. 2000, *A&A*, 353, 498  
 Dupke, R. A. & White R. 2000a, *ApJ*, 528, 139  
 Dupke, R. A. & White R. 2000b, *ApJ*, 537, 123  
 Ettori, S., Allen, S. W., Fabian, A. C. 2001, *MNRAS*, 322, 187  
 Finoguenov, A., David, L. P., Ponman, T. J. 2000, *ApJ*, 544, 188  
 Finoguenov, A., Matsushita, K., Böhringer, H., Ikebe, Y., Arnaud, M. 2001, *A&A* in press, (astro-ph/0110516)  
 Fukazawa, Y., Makishima, K., Tamura, T., Ezawa, H., Xu, H., Ikebe, Y., Kikuchi, K., Ohashi, T. 1998, *PASJ*, 50, 187  
 Gibson, B. K., Lowenstein, M., Mushotzky, R. F. 1997, *MNRAS*, 290, 623  
 Graham, J.A., 1998, *ApJ*, 502, 245  
 Grevesse, N. & Sauval, A. J., 1998, *Space Science Reviews*, 85, 161  
 Guainazzi, M. & Molendi, S. 2000, *A&A*, 351, L19  
 Gunn, J. E. & Gott, J. R. 1972, *ApJ*, 176, 1  
 Hatano, K., Branch, D., Lents, E.J., Baron, E., Filippenko, A.V., Garnavich, P.M., 2000, *ApJ*, 543, L9  
 Hwang, U., Mushotzky R., Lowenstein, M., Markert, T. H., Fukazawa, Y., Matsumoto, H. 1997, *ApJ*, 476, 560  
 Kauffmann, G. & Charlot, S. 1998, *MNRAS*, 294, 705  
 Koekemoer, A.M., O'Dea, C.P., Sarazin, C.L., McNamara, B.R., Donahue, M., Voit, G.M., Baum, S.A., Gallimore, J.F., *ApJ*, 525, 621  
 Jansen, F., Lumb, D., Altieri, B., Clavel, J., Ehle, M., Erd, C., Gabriel, C., Guainazzi, M., Gondoin, P., Much, R., Munoz, R., Santos, M., Scharlet, N., Texier, D., Vacanti, G. 2001, *A&A*, 365, L1  
 Ishimaru, Y. & Arimoto, N. 1997, *PASJ*, 49, 1  
 Liedahl, D. A., Osterheld A. L., Goldstein, W. H. 1995, *ApJ*, 438, L115  
 Lieu, R., Mittaz, J. P. D., Bowyer, S., Lockman, F. J., Hwang, C. Y., Schmitt, J. H. M. 1996, *ApJ*, 458, L5  
 Makishima, K., Ezawa, H., Fukazawa, Y., Honda, H., Ikebe, Y., Kamae, T., Kikuchi, K., Matsushita, K., Nakazawa, K., Ohashi, T., Takahashi, T., Tamura, T., Xu, H. 2001, *PASJ*, 53, 401  
 Matsumoto, H., Koyama, K., Awaki, H., Tomida, H., Tsuru, T., Mushotzky, R., Hatsukade, I. 1996, *PASJ*, 48, 201  
 Matteucci, F. & Vettolani, G. 1988, *A&A*, 202, 21  
 McNamara 1999, presented at "Life cycles of Radio Galaxies", July 15-17, 1999, STScI, Baltimore (astro-ph/9911129)  
 Mewe, R., Gronenschild, E. H. B. M., van den Oord, G. H. J., 1985, *A&AS*, 62, 197  
 Molendi, S. *Report on MOS PN cross-calibration presented at Leicester EPIC calibration meeting held in June 2001*  
 Molendi, S. & Gastaldello, F. 2001, *A&A*, 375, L14  
 Molendi, S. & Pizzolato, F. 2001, *ApJ*, 560, 194  
 Mushotzky, R., Lowenstein, M., Arnaud, K. A., Tamura, T., Fukazawa, Y., Matsushita, K., Kikuchi, K., Hatsukade, I. 1996, *ApJ*, 466, 686  
 Mushotzky, R. & Lowenstein, M. 1997, *ApJ*, 481, L63  
 Nomoto, K., Iwamoto, K., Nakasato, N., Thielemann, F. K., Brachwitz, F., Tsujimoto, T., Kubo, Y., Kishimoto, N. 1997, *Nucl.Phys. A*, 621, 467  
 Nulsen, P.E.J. & Böhringer, H., 1995, *MNRAS*, 274, 1093  
 Renzini, A., 1997, *ApJ*, 488, 35  
 Smith, R. K., Brickhouse, N. S., Liedahl, D. A., Raymond, J. C. 2001, *ApJ*, 556, L91

- Tamura, T., Bleeker, A.M., Kaastra, J.S., Ferrigno, C., Molendi, S. 2001, A&A, 379, 107
- Thomas, P.A. & Fabian, A.C., 1990, MNRAS, 246, 156
- Tonazzo, T. & Schindler, S. 2001, MNRAS, 325, 509
- van Breugel, W.J.M., Heckman, T., Miley, G. 1984, ApJ, 276, 79
- van Breugel, W.J.M., Filippenko, A.V., Heckman, T., Miley, G. 1985, ApJ, 293, 83
- van Breugel, W.J.M. & Dey, A. 1993, ApJ, 414, 563

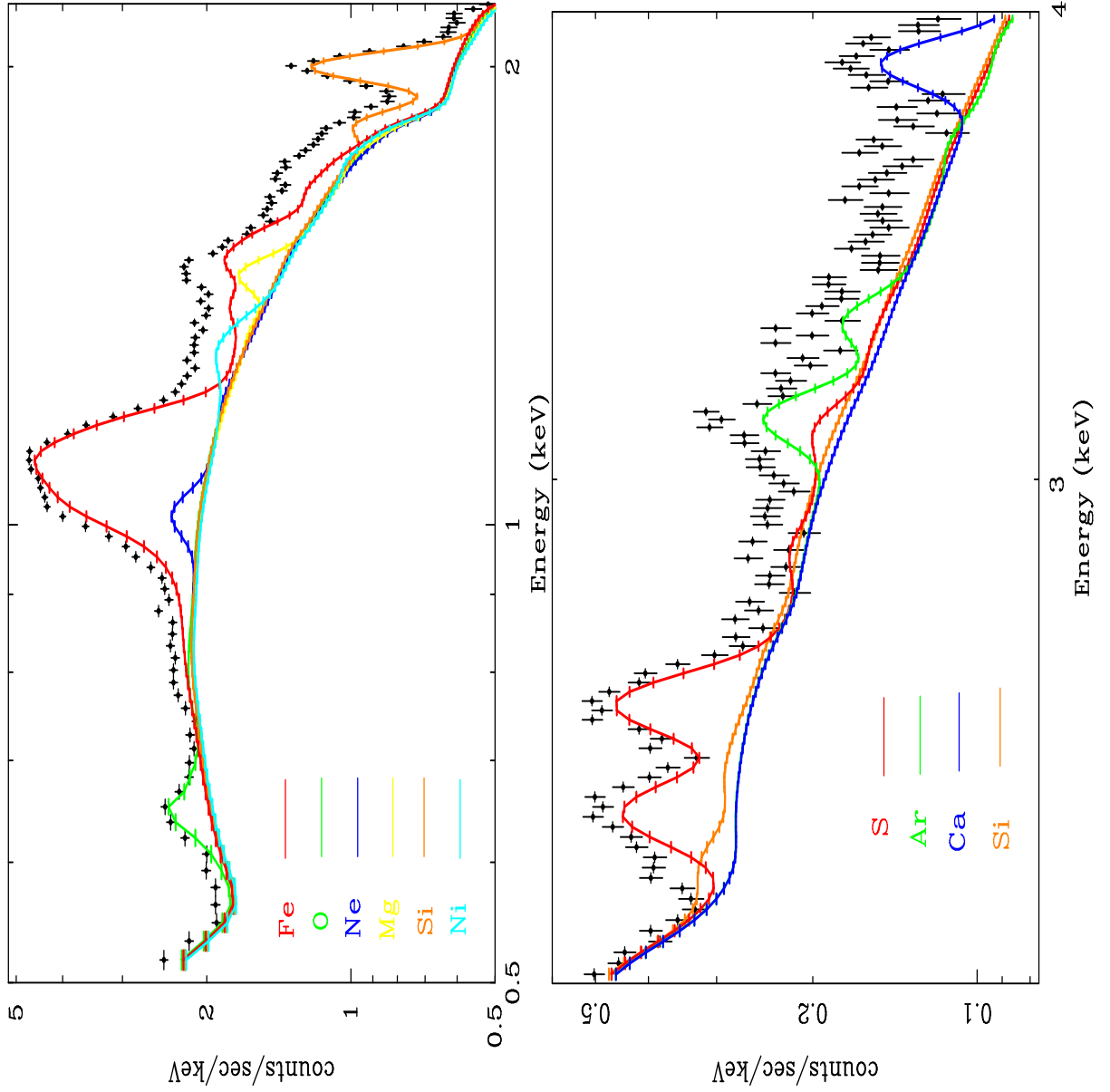


FIG. 1.— Data of the 3'-4' bin and lines of the various elements, obtained by setting all element abundances to zero except the one of interest, calculated using the MEKAL code. **Top Panel:** the lines of O, Fe, Ne, Ni, Mg and Si used for the analysis in the 0.5-2 keV energy range. **Bottom Panel:** the lines of Si, S, Ar and Ca used for the analysis in the 2-4 keV energy range.

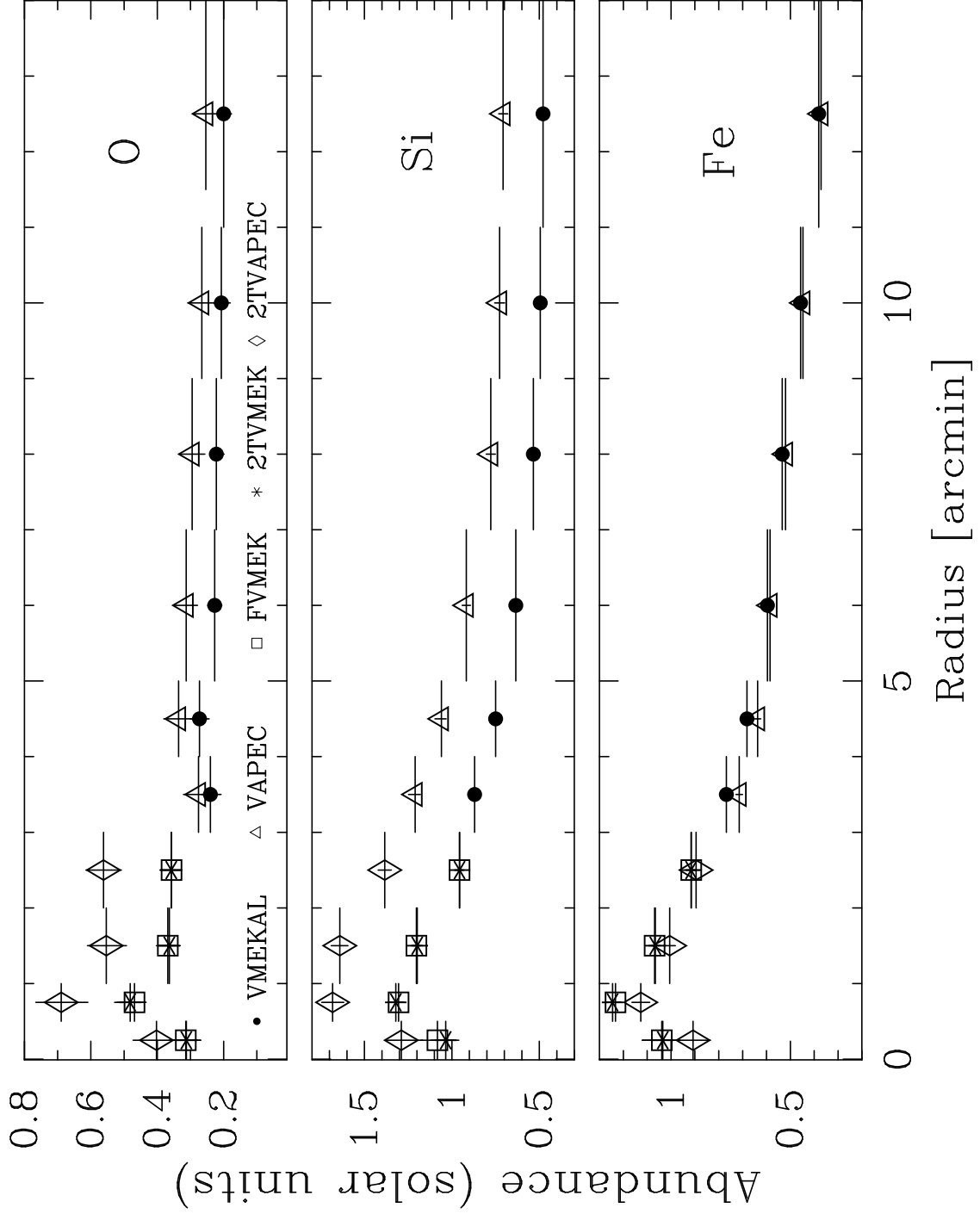


FIG. 2.— MOS abundance profiles for O, Si and Fe. Uncertainties are at the 68% level for one interesting parameter ( $\Delta\chi^2 = 1$ ). Diamonds represent measurements with 2T model using APEC code, asterisks those with 2T model using MEKAL code and squares those with fake multi-phase model using MEKAL code. Full circles indicate measurements with 1T model using MEKAL code while empty triangles those with 1T model using APEC code.



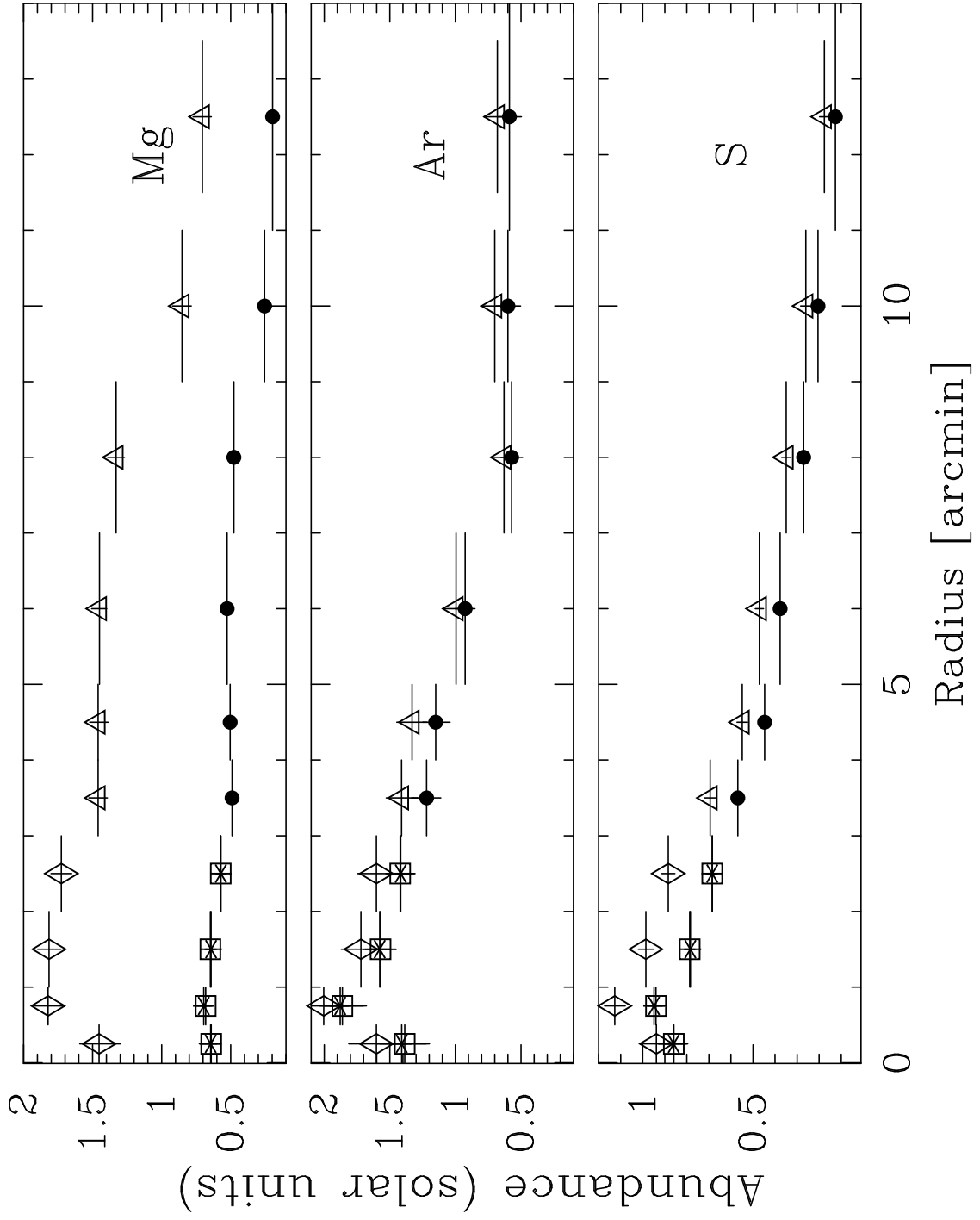


FIG. 3.— MOS abundance profiles for Mg, Ar and S. Symbols as in Figure 2.

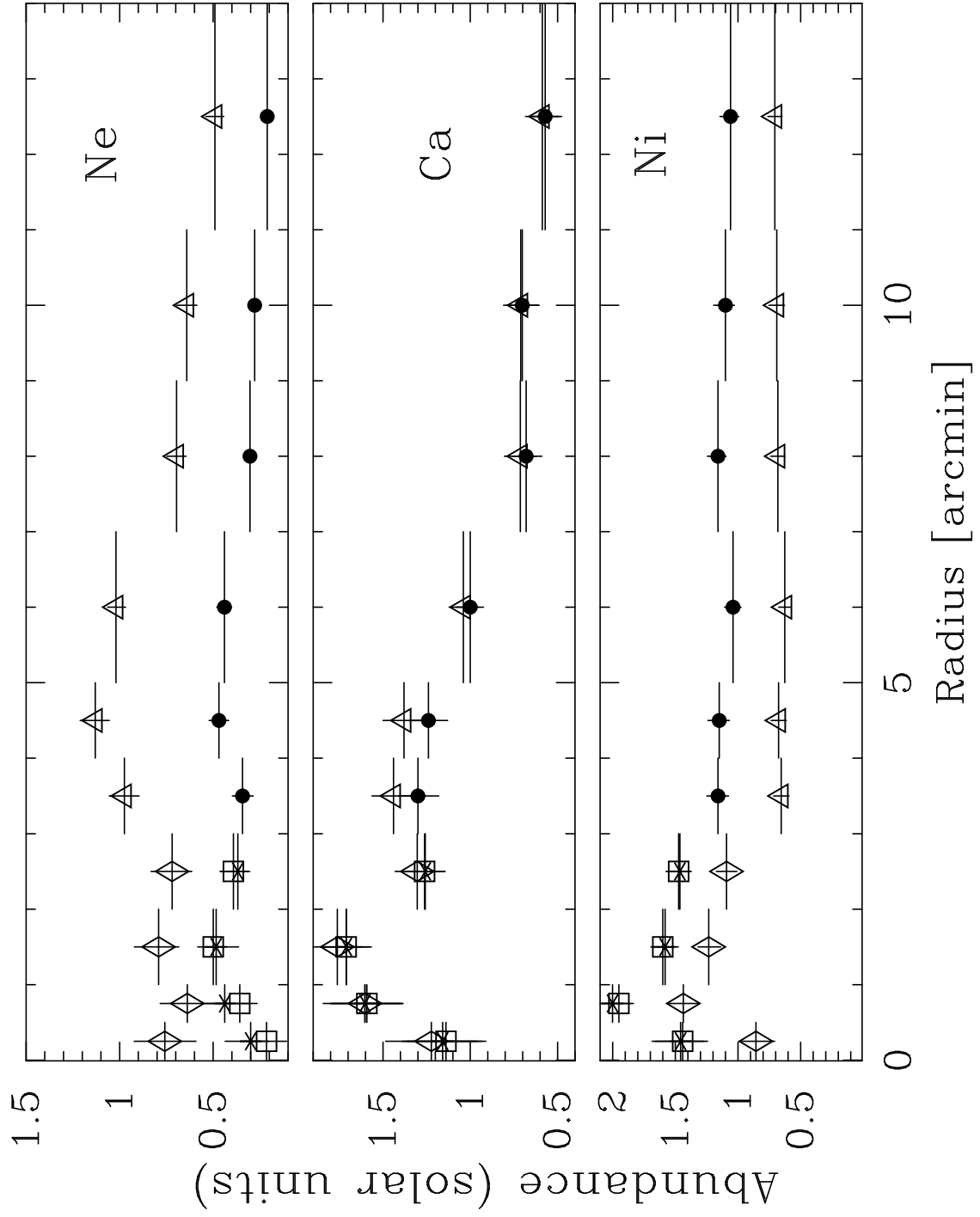


FIG. 4.— MOS abundance profiles for Ne, Ca and Ni. Symbols as in Figure 3.

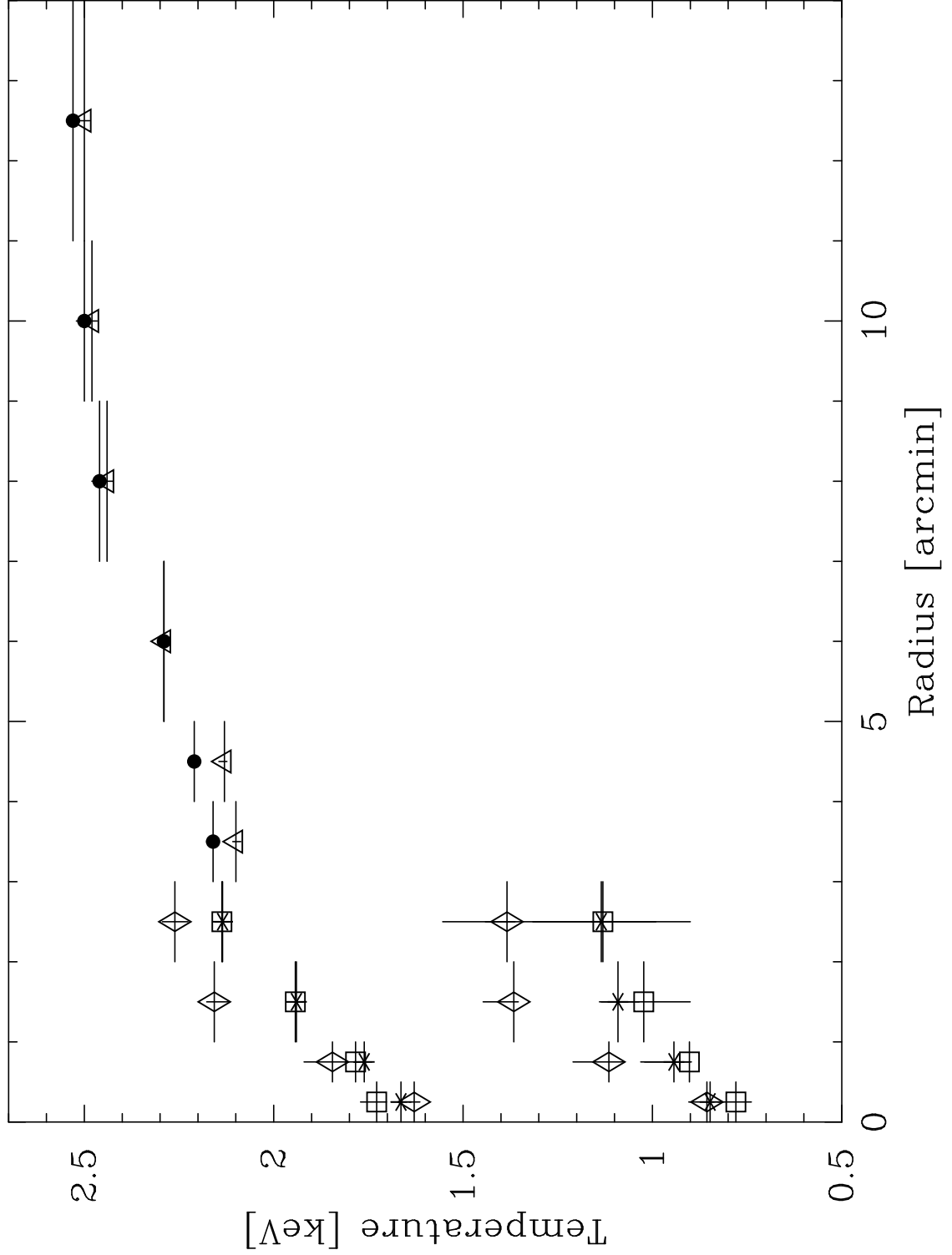


FIG. 5.— MOS temperature profile. Uncertainties are at the 68% level for one interesting parameter ( $\Delta\chi^2 = 1$ ). Diamonds and asterisks represent the two temperature values obtained with 2T models using APEC code and MEKAL code, respectively. Squares represent the value of the temperature of the vmekal component and the  $T_{min}$  of the vmcflow component, for the fake multi-phase model using MEKAL code. Full circles indicate temperature obtained with 1T model using MEKAL code while empty triangles those with 1T model using APEC code.

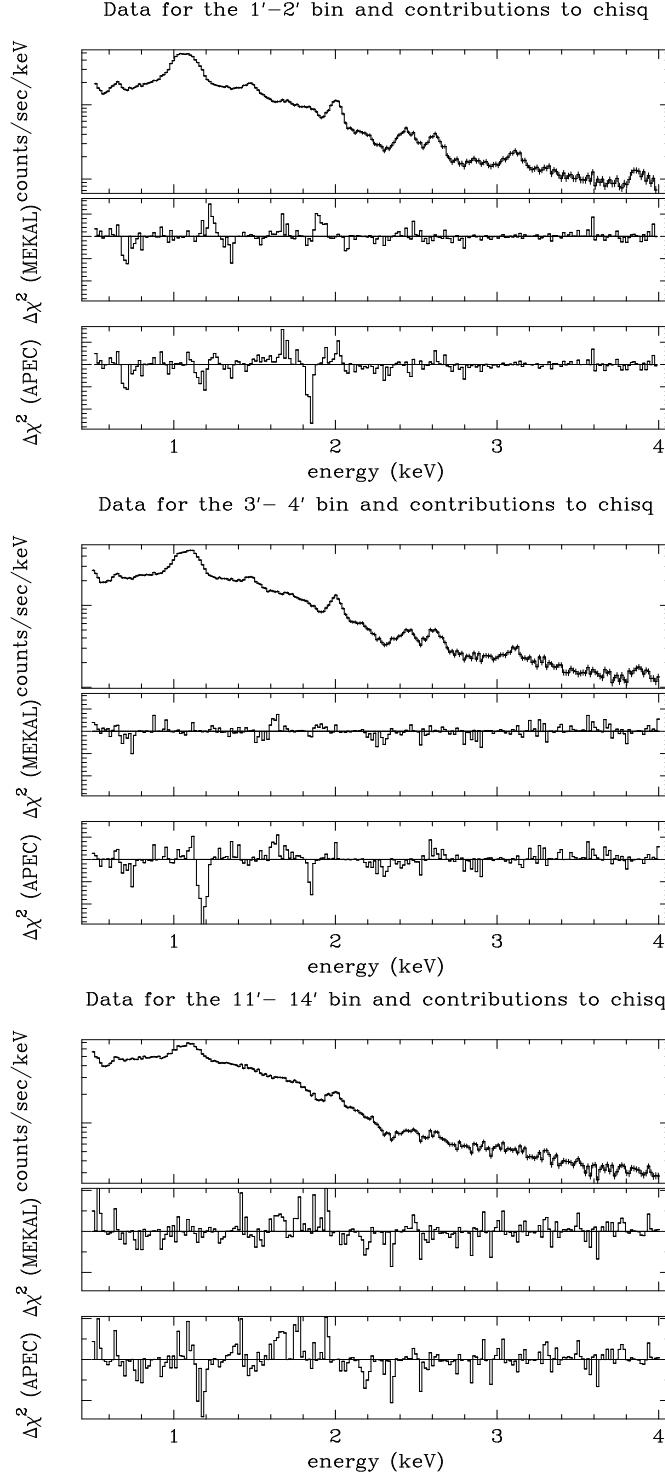


FIG. 6.— **Top Panel:** data for the bin 1'-2' and contributions to  $\chi^2$  for a 2T model with MEKAL code, the  $\chi^2/d.o.f.$  of the fit is 381/217, and for a 2T model with APEC code, the  $\chi^2/d.o.f.$  of the fit is 474/218. Contributions to  $\chi^2$  are on the same scale for direct comparison.

**Middle Panel:** data for the bin 3'-4' and contributions to  $\chi^2$  for a 1T model with MEKAL code, the  $\chi^2/d.o.f.$  of the fit is 326/221, and for a 1T model with APEC code, the  $\chi^2/d.o.f.$  of the fit is 546/222. Contributions to  $\chi^2$  are on the same scale for direct comparison.

**Bottom Panel:** data for the bin 11'-14' and contributions to  $\chi^2$  for a 1T model with MEKAL code, the  $\chi^2/d.o.f.$  of the fit is 729/221, and for a 1T model with APEC code, the  $\chi^2/d.o.f.$  of the fit is 886/222. Contributions to  $\chi^2$  are on the same scale for direct comparison.

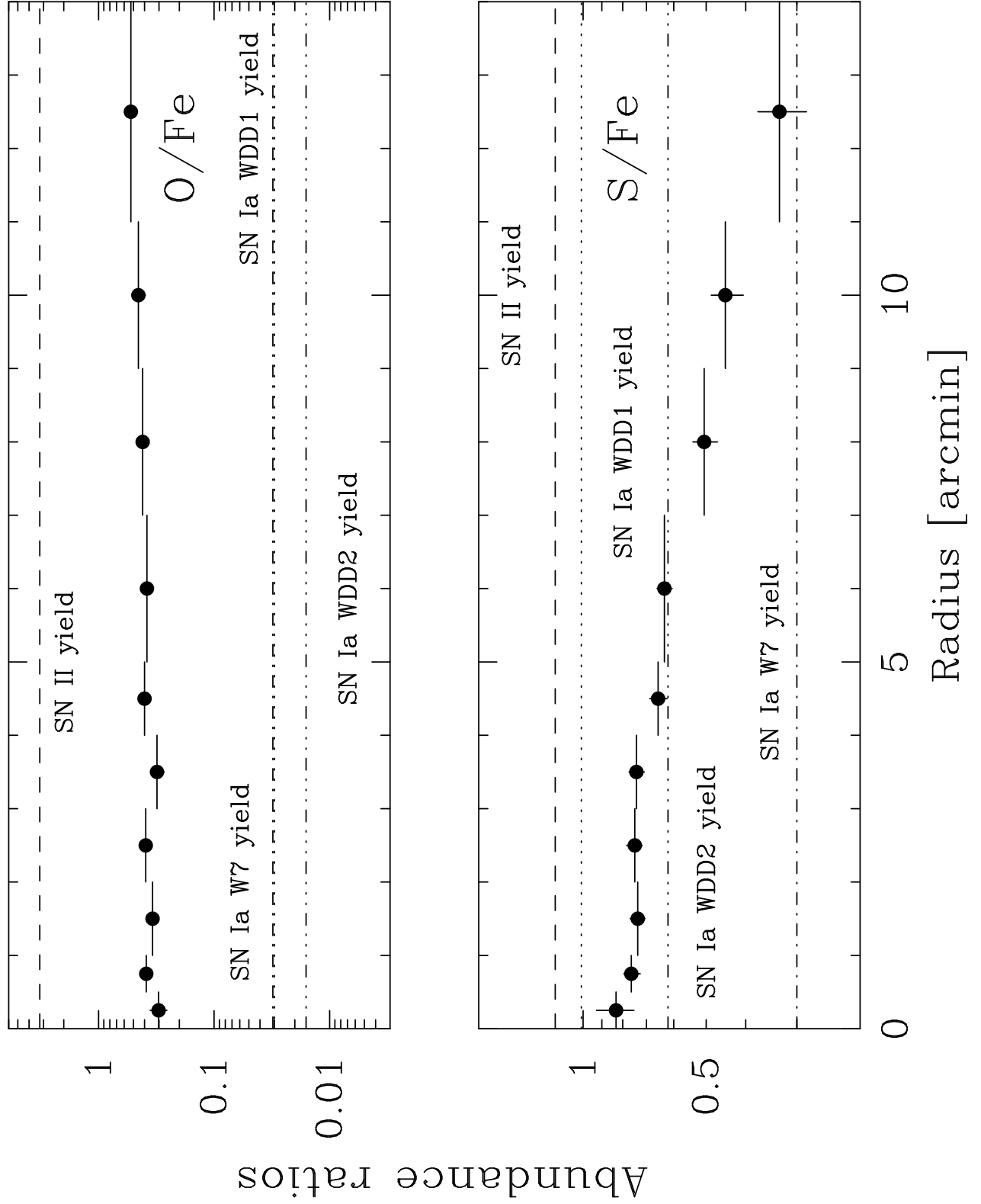


FIG. 7.— MOS abundance ratio profiles for  $O/Fe$  and  $S/Fe$ . Also showed are the abundance ratios predicted by SNe models taken by Nomoto et al. (1997): the dashed line refers to the SNII model, the dash-dotted line to the W7 SNIa model, the dotted line to the WDD1 SNIa model and the three dotted-dashed line to the WDD2 SNIa model.

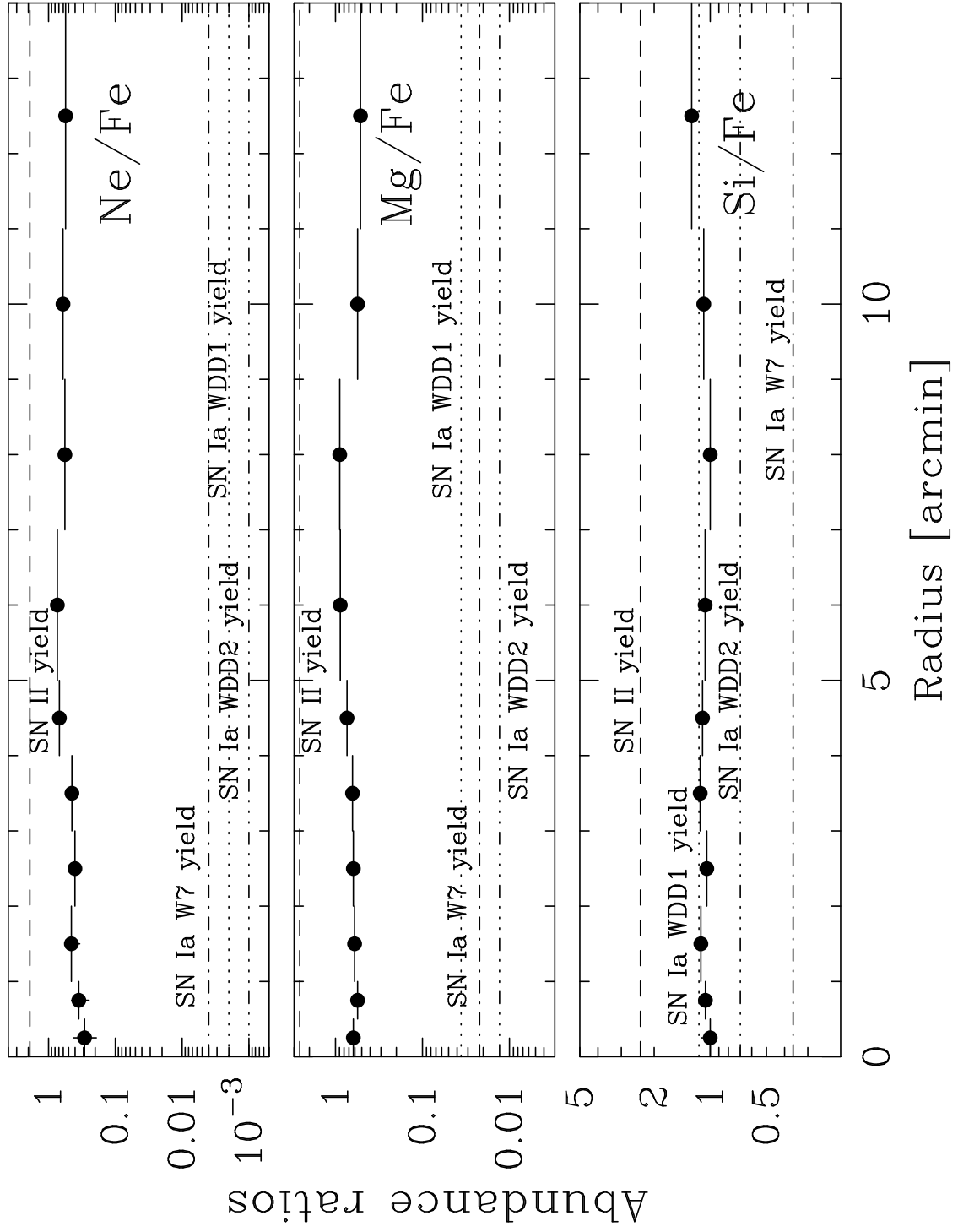


FIG. 8.— Same as Figure 7 but for ratio profiles for Ne/Fe, Mg/Fe and Si/Fe

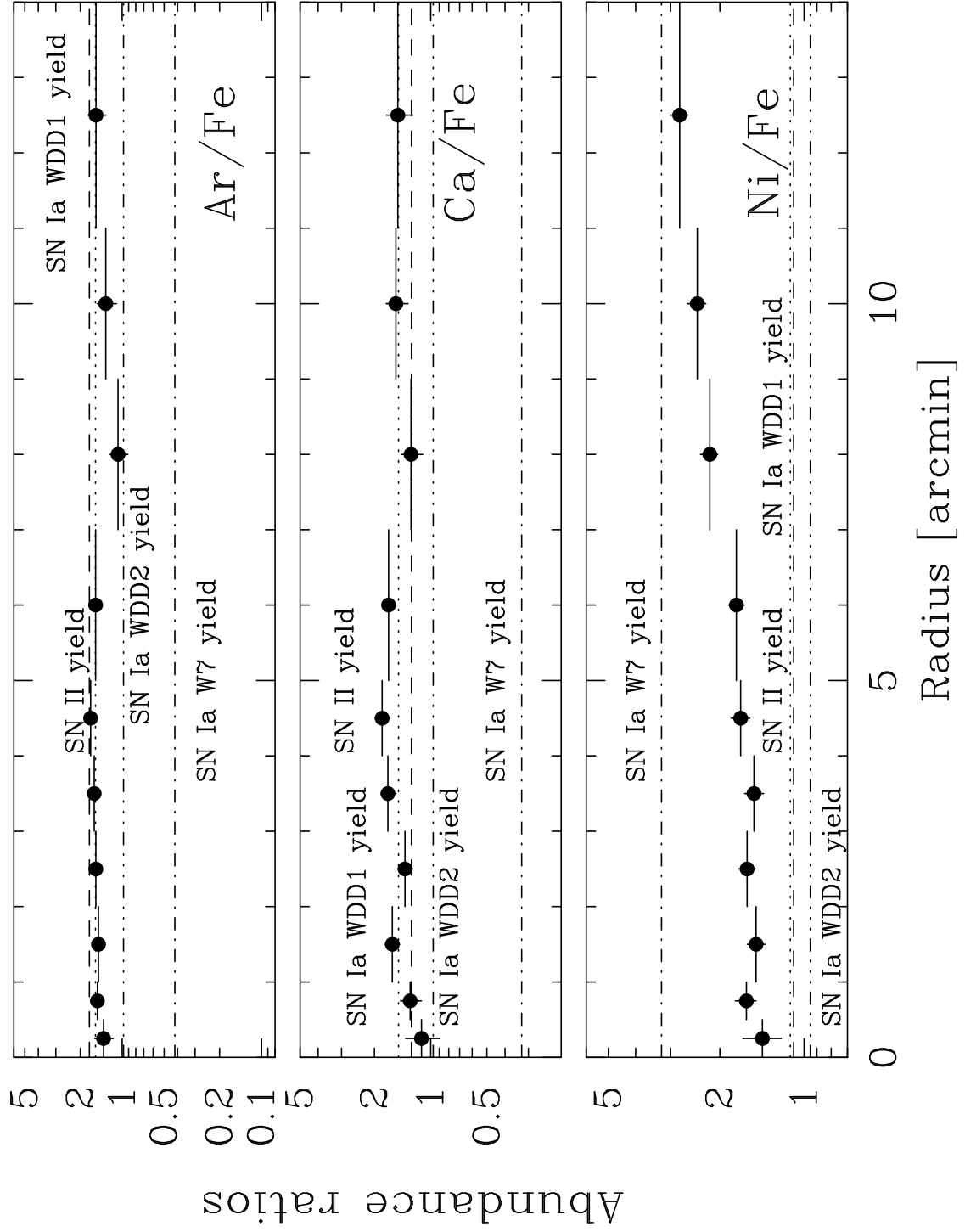


FIG. 9.— Same as Figure 7 but for ratio profiles for Ar/Fe, Ca/Fe and Ni/Fe.

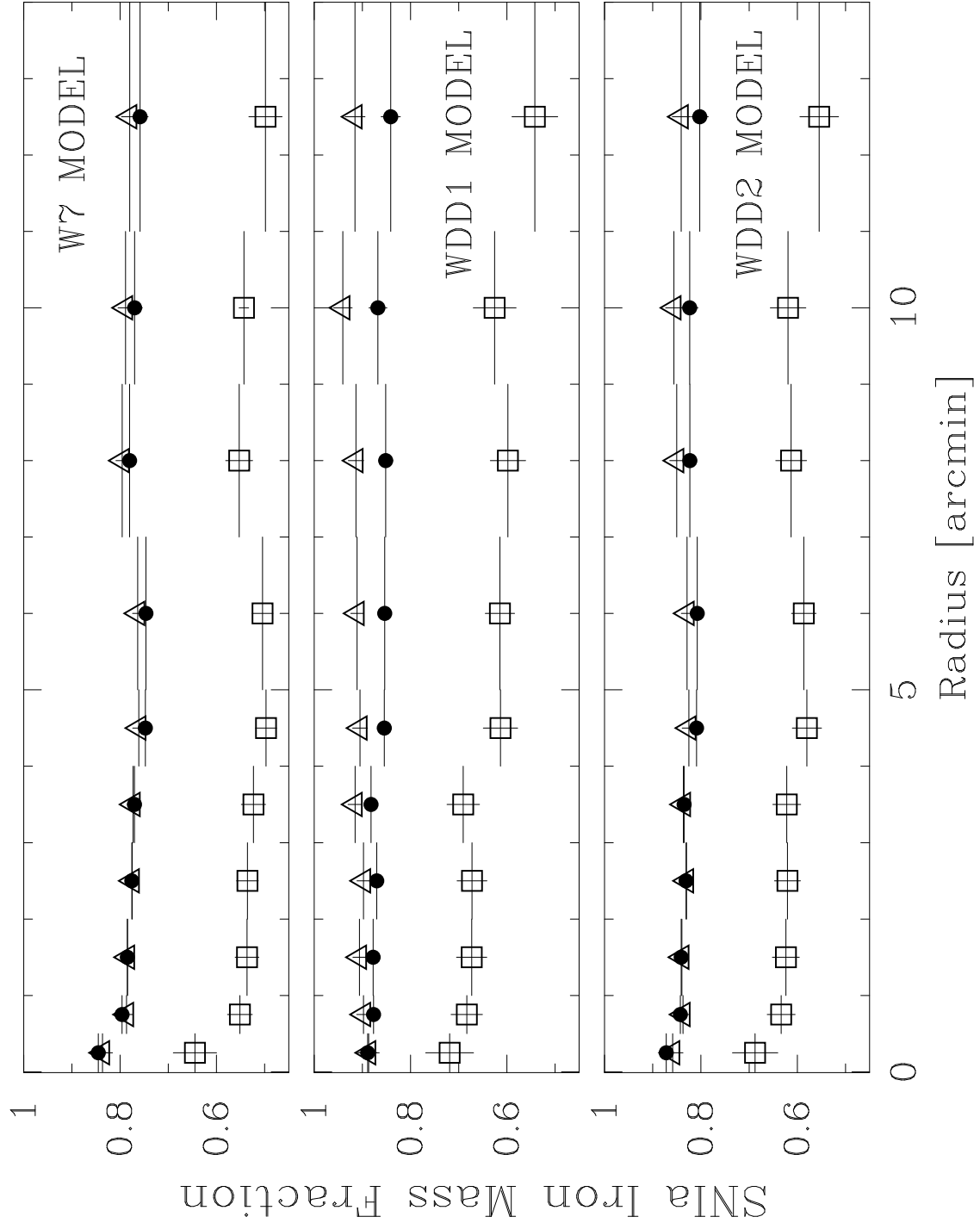


FIG. 10.— **Top Panel** SN Ia Fe Mass Fraction obtained by a simultaneous fit of the eight abundance ratios of Table 2, using the W7 model for SN Ia and different yields for SN II: the ones by Nomoto et al.(1997) (circles), the upper end of the range indicated by Gibson et al.(1997) (triangles) and the lower end of the range (squares). Errors are at 68% confidence limit( $1\sigma$ ).

**Middle Panel** Same as the top panel but using WDD1 model for SN Ia.

**Bottom Panel** Same as the top panel but using WDD2 model for SN Ia.



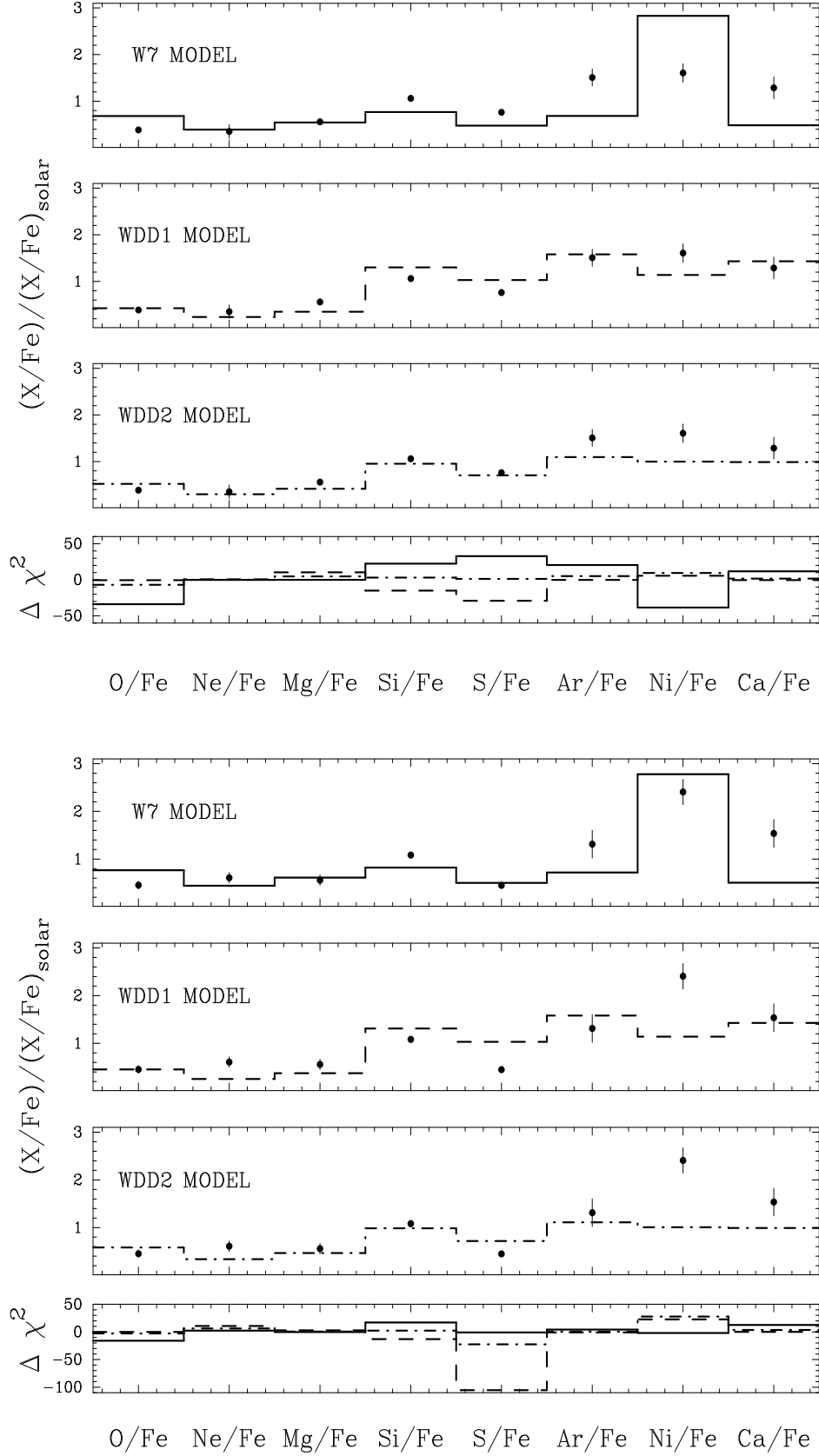


FIG. 11.— **Top Panel** Abundance ratios for the 0.5'-1' bin, best fits for the Nomoto SNIa models, in combination with the Nomoto SNII model, and contributions to  $\chi^2$  for the various models. The solid line refers to the W7 model, the dashed line to the WDD1 model and the dot-dashed line to the WDD2 model. **Bottom Panel** Same as the top panel but for the 11'-14' bin.

TABLE 1

ABUNDANCE PROFILES OBTAINED BY A 2T VMEKAL MODELING FOR THE CENTRAL REGIONS AND A 1T VMEKAL MODELING FOR THE OUTER REGIONS. ALL ABUNDANCES REFERRED TO SOLAR UNITS AS GIVEN IN GREVESSE & SAUVAL (1998). ALL ERRORS QUOTED ARE AT THE 68% LEVEL FOR ONE INTERESTING PARAMETER ( $\Delta\chi^2 = 1$ )

Bin	O	Ne	Mg	Si	S	Ar	Ca	Fe	Ni
0'-0.5'	0.31 <sup>+0.05</sup> <sub>-0.04</sub>	0.30 <sup>+0.14</sup> <sub>-0.10</sub>	0.64 <sup>+0.08</sup> <sub>-0.05</sub>	1.03 <sup>+0.08</sup> <sub>-0.07</sub>	0.86 <sup>+0.07</sup> <sub>-0.06</sub>	1.41 <sup>+0.19</sup> <sub>-0.19</sub>	1.16 <sup>+0.23</sup> <sub>-0.22</sub>	1.03 <sup>+0.08</sup> <sub>-0.07</sub>	1.46 <sup>+0.23</sup> <sub>-0.18</sub>
0.5'-1'	0.48 <sup>+0.04</sup> <sub>-0.05</sub>	0.44 <sup>+0.12</sup> <sub>-0.13</sub>	0.69 <sup>+0.05</sup> <sub>-0.06</sub>	1.32 <sup>+0.04</sup> <sub>-0.04</sub>	0.95 <sup>+0.03</sup> <sub>-0.04</sub>	1.88 <sup>+0.12</sup> <sub>-0.18</sub>	1.60 <sup>+0.20</sup> <sub>-0.20</sub>	1.24 <sup>+0.03</sup> <sub>-0.04</sub>	2.00 <sup>+0.19</sup> <sub>-0.14</sub>
1'-2'	0.36 <sup>+0.04</sup> <sub>-0.03</sub>	0.48 <sup>+0.10</sup> <sub>-0.12</sub>	0.64 <sup>+0.04</sup> <sub>-0.04</sub>	1.20 <sup>+0.03</sup> <sub>-0.03</sub>	0.78 <sup>+0.03</sup> <sub>-0.02</sub>	1.58 <sup>+0.12</sup> <sub>-0.13</sub>	1.71 <sup>+0.14</sup> <sub>-0.14</sub>	1.07 <sup>+0.03</sup> <sub>-0.02</sub>	1.58 <sup>+0.11</sup> <sub>-0.11</sub>
2'-3'	0.36 <sup>+0.03</sup> <sub>-0.03</sub>	0.37 <sup>+0.09</sup> <sub>-0.06</sub>	0.57 <sup>+0.03</sup> <sub>-0.04</sub>	0.96 <sup>+0.03</sup> <sub>-0.03</sub>	0.68 <sup>+0.03</sup> <sub>-0.02</sub>	1.42 <sup>+0.11</sup> <sub>-0.11</sub>	1.26 <sup>+0.11</sup> <sub>-0.11</sub>	0.92 <sup>+0.02</sup> <sub>-0.02</sub>	1.46 <sup>+0.10</sup> <sub>-0.09</sub>
3'-4'	0.24 <sup>+0.03</sup> <sub>-0.03</sub>	0.34 <sup>+0.05</sup> <sub>-0.06</sub>	0.49 <sup>+0.03</sup> <sub>-0.04</sub>	0.87 <sup>+0.02</sup> <sub>-0.02</sub>	0.57 <sup>+0.02</sup> <sub>-0.02</sub>	1.22 <sup>+0.11</sup> <sub>-0.11</sub>	1.30 <sup>+0.11</sup> <sub>-0.12</sub>	0.77 <sup>+0.01</sup> <sub>-0.02</sub>	1.16 <sup>+0.09</sup> <sub>-0.08</sub>
4'-5'	0.27 <sup>+0.03</sup> <sub>-0.03</sub>	0.47 <sup>+0.05</sup> <sub>-0.05</sub>	0.50 <sup>+0.03</sup> <sub>-0.03</sub>	0.75 <sup>+0.02</sup> <sub>-0.02</sub>	0.45 <sup>+0.02</sup> <sub>-0.02</sub>	1.15 <sup>+0.10</sup> <sub>-0.11</sub>	1.24 <sup>+0.11</sup> <sub>-0.11</sub>	0.68 <sup>+0.01</sup> <sub>-0.01</sub>	1.15 <sup>+0.09</sup> <sub>-0.08</sub>
5'-7'	0.23 <sup>+0.02</sup> <sub>-0.02</sub>	0.44 <sup>+0.04</sup> <sub>-0.04</sub>	0.53 <sup>+0.03</sup> <sub>-0.03</sub>	0.63 <sup>+0.02</sup> <sub>-0.01</sub>	0.38 <sup>+0.01</sup> <sub>-0.01</sub>	0.93 <sup>+0.07</sup> <sub>-0.07</sub>	1.00 <sup>+0.08</sup> <sub>-0.07</sub>	0.60 <sup>+0.01</sup> <sub>-0.01</sub>	1.04 <sup>+0.07</sup> <sub>-0.06</sub>
7'-9'	0.22 <sup>+0.02</sup> <sub>-0.02</sub>	0.30 <sup>+0.03</sup> <sub>-0.03</sub>	0.48 <sup>+0.03</sup> <sub>-0.03</sub>	0.53 <sup>+0.02</sup> <sub>-0.02</sub>	0.27 <sup>+0.01</sup> <sub>-0.01</sub>	0.57 <sup>+0.08</sup> <sub>-0.08</sub>	0.68 <sup>+0.08</sup> <sub>-0.09</sub>	0.53 <sup>+0.02</sup> <sub>-0.02</sub>	1.16 <sup>+0.08</sup> <sub>-0.06</sub>
9'-11'	0.21 <sup>+0.02</sup> <sub>-0.03</sub>	0.28 <sup>+0.03</sup> <sub>-0.03</sub>	0.25 <sup>+0.03</sup> <sub>-0.03</sub>	0.49 <sup>+0.02</sup> <sub>-0.02</sub>	0.20 <sup>+0.02</sup> <sub>-0.02</sub>	0.60 <sup>+0.09</sup> <sub>-0.10</sub>	0.70 <sup>+0.09</sup> <sub>-0.10</sub>	0.46 <sup>+0.01</sup> <sub>-0.01</sub>	1.10 <sup>+0.09</sup> <sub>-0.07</sub>
11'-14'	0.20 <sup>+0.02</sup> <sub>-0.02</sub>	0.21 <sup>+0.03</sup> <sub>-0.03</sub>	0.20 <sup>+0.03</sup> <sub>-0.03</sub>	0.48 <sup>+0.02</sup> <sub>-0.01</sub>	0.13 <sup>+0.02</sup> <sub>-0.02</sub>	0.59 <sup>+0.08</sup> <sub>-0.09</sub>	0.57 <sup>+0.09</sup> <sub>-0.09</sub>	0.38 <sup>+0.01</sup> <sub>-0.01</sub>	1.06 <sup>+0.08</sup> <sub>-0.07</sub>

TABLE 2

ABUNDANCE RATIOS FROM OUR RESULTS AND FROM SNe MODELS. THE ABUNDANCES RELATIVE TO Fe NORMALIZED TO THE SOLAR VALUE,  $(X/Fe)/(X_{\odot}/Fe_{\odot})$ , WHERE X AND Fe ARE NUMBER DENSITY OF THE ELEMENT AND Fe, ARE SHOWN. THE ERRORS ASSOCIATED WITH THE OBSERVED ABUNDANCE RATIOS ARE THE PROPAGATED  $1\sigma$  ERRORS.

	O	Ne	Mg	Si	S	Ar	Ca	Ni
0'-0.5'	0.30 <sup>+0.06</sup> <sub>-0.04</sub>	0.29 <sup>+0.13</sup> <sub>-0.10</sub>	0.62 <sup>+0.09</sup> <sub>-0.06</sub>	1.00 <sup>+0.12</sup> <sub>-0.10</sub>	0.83 <sup>+0.10</sup> <sub>-0.08</sub>	1.36 <sup>+0.21</sup> <sub>-0.20</sub>	1.12 <sup>+0.24</sup> <sub>-0.23</sub>	1.41 <sup>+0.25</sup> <sub>-0.20</sub>
0.5'-1'	0.39 <sup>+0.03</sup> <sub>-0.04</sub>	0.35 <sup>+0.10</sup> <sub>-0.10</sub>	0.56 <sup>+0.04</sup> <sub>-0.05</sub>	1.06 <sup>+0.04</sup> <sub>-0.05</sub>	0.76 <sup>+0.03</sup> <sub>-0.04</sub>	1.51 <sup>+0.10</sup> <sub>-0.15</sub>	1.29 <sup>+0.16</sup> <sub>-0.17</sub>	1.61 <sup>+0.15</sup> <sub>-0.12</sub>
1'-2'	0.34 <sup>+0.04</sup> <sub>-0.03</sub>	0.45 <sup>+0.09</sup> <sub>-0.11</sub>	0.60 <sup>+0.04</sup> <sub>-0.04</sub>	1.12 <sup>+0.04</sup> <sub>-0.05</sub>	0.73 <sup>+0.03</sup> <sub>-0.03</sub>	1.48 <sup>+0.12</sup> <sub>-0.12</sub>	1.60 <sup>+0.14</sup> <sub>-0.14</sub>	1.48 <sup>+0.11</sup> <sub>-0.10</sub>
2'-3'	0.39 <sup>+0.04</sup> <sub>-0.03</sub>	0.40 <sup>+0.10</sup> <sub>-0.07</sub>	0.62 <sup>+0.04</sup> <sub>-0.04</sub>	1.04 <sup>+0.04</sup> <sub>-0.04</sub>	0.75 <sup>+0.03</sup> <sub>-0.03</sub>	1.55 <sup>+0.12</sup> <sub>-0.12</sub>	1.37 <sup>+0.13</sup> <sub>-0.13</sub>	1.60 <sup>+0.12</sup> <sub>-0.11</sub>
3'-4'	0.31 <sup>+0.04</sup> <sub>-0.04</sub>	0.45 <sup>+0.07</sup> <sub>-0.07</sub>	0.64 <sup>+0.04</sup> <sub>-0.06</sub>	1.13 <sup>+0.04</sup> <sub>-0.04</sub>	0.74 <sup>+0.03</sup> <sub>-0.03</sub>	1.59 <sup>+0.15</sup> <sub>-0.14</sub>	1.69 <sup>+0.15</sup> <sub>-0.16</sub>	1.51 <sup>+0.12</sup> <sub>-0.11</sub>
4'-5'	0.40 <sup>+0.04</sup> <sub>-0.04</sub>	0.69 <sup>+0.08</sup> <sub>-0.08</sub>	0.74 <sup>+0.05</sup> <sub>-0.05</sub>	1.10 <sup>+0.04</sup> <sub>-0.04</sub>	0.65 <sup>+0.03</sup> <sub>-0.03</sub>	1.69 <sup>+0.15</sup> <sub>-0.16</sub>	1.82 <sup>+0.16</sup> <sub>-0.16</sub>	1.69 <sup>+0.14</sup> <sub>-0.12</sub>
5'-7'	0.38 <sup>+0.04</sup> <sub>-0.04</sub>	0.74 <sup>+0.07</sup> <sub>-0.06</sub>	0.88 <sup>+0.05</sup> <sub>-0.05</sub>	1.06 <sup>+0.03</sup> <sub>-0.03</sub>	0.63 <sup>+0.03</sup> <sub>-0.03</sub>	1.55 <sup>+0.13</sup> <sub>-0.13</sub>	1.68 <sup>+0.13</sup> <sub>-0.13</sub>	1.74 <sup>+0.12</sup> <sub>-0.11</sub>
7'-9'	0.41 <sup>+0.04</sup> <sub>-0.04</sub>	0.57 <sup>+0.06</sup> <sub>-0.06</sub>	0.89 <sup>+0.07</sup> <sub>-0.06</sub>	1.00 <sup>+0.05</sup> <sub>-0.04</sub>	0.50 <sup>+0.03</sup> <sub>-0.04</sub>	1.07 <sup>+0.15</sup> <sub>-0.16</sub>	1.27 <sup>+0.16</sup> <sub>-0.17</sub>	2.17 <sup>+0.17</sup> <sub>-0.14</sub>
9'-11'	0.45 <sup>+0.05</sup> <sub>-0.06</sub>	0.61 <sup>+0.08</sup> <sub>-0.08</sub>	0.56 <sup>+0.08</sup> <sub>-0.07</sub>	1.08 <sup>+0.04</sup> <sub>-0.04</sub>	0.45 <sup>+0.04</sup> <sub>-0.04</sub>	1.31 <sup>+0.19</sup> <sub>-0.21</sub>	1.54 <sup>+0.20</sup> <sub>-0.21</sub>	2.41 <sup>+0.21</sup> <sub>-0.16</sub>
11'-14'	0.52 <sup>+0.05</sup> <sub>-0.06</sub>	0.55 <sup>+0.07</sup> <sub>-0.08</sub>	0.52 <sup>+0.09</sup> <sub>-0.09</sub>	1.26 <sup>+0.05</sup> <sub>-0.04</sub>	0.33 <sup>+0.04</sup> <sub>-0.05</sub>	1.54 <sup>+0.22</sup> <sub>-0.24</sub>	1.50 <sup>+0.23</sup> <sub>-0.25</sub>	2.78 <sup>+0.22</sup> <sub>-0.18</sub>
W7 <sup>a</sup>	0.031	0.004	0.022	0.36	0.30	0.42	0.33	3.23
WDD1 <sup>a</sup>	0.030	0.002	0.036	1.15	1.01	1.56	1.48	1.12
WDD2 <sup>a</sup>	0.016	0.001	0.013	0.69	0.62	0.98	0.97	0.95
SNII <sup>b</sup>	3.23	1.90	2.58	2.37	1.17	1.72	1.09	1.27
SNII <sup>c</sup>	1.25-2.80	0.96-1.93	0.96-1.89	1.81-2.54	0.85-2.08	-	-	-

<sup>a</sup> Different models of SNIa taken by Nomoto et al. (1997).

<sup>b</sup> Yields of SNII taken by Nomoto et al. (1997).

<sup>c</sup> Gibson et al. (1997) who choose a representative sample of SNII yields in literature.